Acta Materialia 98 (2015) 141–151

Contents lists available at ScienceDirect

Acta Materialia

journal homepage: www.elsevier.com/locate/actamat

Developing strength and toughness in bio-inspired silicon carbide hybrid materials containing a compliant phase

Valentina Naglieri [a], Bernd Gludovatz [a], Antoni P. Tomsia [a], Robert O. Ritchie [a,b,*]

[a] *Materials Sciences Division, Lawrence Berkeley National Laboratory, Berkeley, CA 94720, USA*
[b] *Department of Materials Science & Engineering, University of California, Berkeley, CA 94720, USA*

ARTICLE INFO

Article history:
Received 29 March 2015
Revised 9 July 2015
Accepted 9 July 2015

Keywords:
Bio-inspired composites
Silicon carbide
PMMA
Damage-tolerance
Freeze casting

ABSTRACT

Freeze casting has proven to be a versatile processing route to fabricate bio-inspired ("nacre-like") hybrid composites that exhibit unique combinations of strength and toughness (damage-tolerance). To date, however, the effects of small changes in the architecture of such composites on their mechanical properties have been poorly investigated. Here we examine the influence of microstructural features such as ceramic/polymer ratio, layer thickness, and presence of bridges between ceramic lamellae, on the mechanical performance of the resulting composites. To this end, we compare the flexural strength and resistance to failure of a suite of silicon carbide/polymethyl methacrylate (SiC/PMMA) layered composites made by polymer infiltration of freeze-cast SiC scaffolds with various architectures. Our composite structures all show an increasing fracture resistance with crack extension (rising R-curve behavior) due to extrinsic toughening mechanisms such as uncracked-ligament bridging, inelastic deformation of ductile layers, lamellae pull out and ceramic bridge fracture. We show that a fine tuning of the composite architecture can lead to SiC/PMMA samples with a dendritic morphology, which exhibit the best strength and toughness. Specifically, the presence of ceramic bridges connecting the lamellae is seen to provide a strengthening effect similar to the mineral bridges between aragonite platelets in nacre, where they prevent debonding and limit platelet sliding; additionally, the fracture of these bridges between lamellae during crack extension is a potent toughening mechanism, thereby conferring optimal damage tolerance to the material.

1. Introduction

The mechanical properties of structural materials, particularly in the quest for tougher and stronger (damage-tolerant) materials, have been an important topic of research for many decades [1]. Although ceramics are often ideal candidate materials when high specific strength, stiffness and creep resistance are required, their inherent brittleness and flaw sensitivity severely limit their potential use for many structural applications.

Natural materials such as nacre, bone or dentin, are biological composites in which highly brittle minerals (hydroxyapatite, aragonite, etc.) and soft biopolymers (collagen, chitin, cellulose, lignin, etc.), are combined in complex hierarchical structures. Despite containing significant amounts of the brittle component, the mechanical properties of these materials, in particular their fracture toughness, are quite exceptional and invariably exceed those of the individual constituents [2]. The excellent fracture resistance of biological composites, however, does not necessarily result from conventional measures of the toughness, such as the *crack-initiation toughness* K_{Ic}, but rather from the fact that these materials can sustain subcritical cracking without catastrophic failure, the latter being a function of their *crack-growth toughness* which can be assessed in terms of so-called rising crack-resistance curve (R-curve) behavior. Such fracture resistance results from a combination of toughening mechanisms that occur both ahead of the crack tip, i.e., intrinsic mechanisms largely associated with plasticity, and those occurring primarily in the wake of a propagating crack, i.e., extrinsic mechanisms associated with crack-tip shielding[1] [3].

---

* Corresponding author at: Department of Materials Science & Engineering, University of California, Berkeley, CA 94720, USA.
E-mail address: roritchie@lbl.gov (R.O. Ritchie).

[1] Intrinsic toughening mechanisms operate ahead of the crack tip to generate resistance to microstructural damage, primarily through plastic deformation which provides a means of blunting the crack tip through the formation of "plastic" zones. Extrinsic toughening mechanisms, conversely, operate primarily in the wake of the crack tip to inhibit cracking by "shielding" the crack from the applied driving force. Whereas intrinsic toughening is effective in inhibiting both the initiation and growth of cracks, extrinsic mechanisms, e.g., crack bridging and crack deflection, are only effective in inhibiting crack growth [1,3].

http://dx.doi.org/10.1016/j.actamat.2015.07.022
1359-6454/

Nacre, the ‘gold standard’ for biomimicry with both high strength and toughness, has been the source of inspiration for many synthetic hybrid materials that aspire to combine strength with deformability [4–9]. Comprising ~95 vol.% of aragonite ($CaCO_3$) platelets surrounded by thin layer of proteins, nacre displays a fracture toughness that is at least one order of magnitude higher than that of either the mineral or the bio-polymers.[2] This result is achieved through a precise architecture that resembles that of a brick wall, and the clever design of the interface. Specifically, hard aragonite platelets as the “bricks” provide for strength and the organic layer as the “mortar” enables *limited* inelastic deformation and thus energy dissipation, yielding a composite, when hydrated, that is remarkably strong (~130 MPa) and tough (work of fracture ~1 kJ m^{-2}) [10]. Nacre’s characteristic brick-and-mortar architecture and the associated toughening mechanisms have been widely studied [10–13] to the extent that the design of nacre-inspired composites is now arguably guided by theoretical models predicting the mechanical response of ideal structures [14–17].

However, enticing as these natural composites are, the development of a new class of damage-tolerant, nature-inspired materials is still surprisingly limited to but a few examples [5–9]; despite some notable results, this field is far from maturity. Although the concepts underlying the design of nacre-inspired materials are quite straightforward [15], the development of such composites is constrained by our ability to make them. Conventional processing techniques, e.g., tape casting and hot pressing [18,19], are unable to replicate the hierarchy observed in natural composites such that toughening is generated mainly from crack deflection rather than concomitant mechanisms acting at multiple length-scales. “Bottom-up” approaches, such as layer-by-layer deposition [20,21], self-assembly [22,23], etc., are often not suitable to fabricate bulk materials and are generally limited to thin films of moderate practical interest. Alternatively, freeze casting (ice-templating) [24] offers the unique opportunity to employ a “top-down” approach to mimic the hierarchical structure of nacre; indeed, to date this processing technique has yielded several bulk hybrid materials with very unique properties [6,8,9,25].

This technique has been exploited to produce scaffolds with complex porosity [24,26–30], and has proven to be effective for the fabrication of nacre-like composites based on alumina [3,6,8,24,25]. By unidirectional freezing of a ceramic suspension, a solid body made of alternate layers of ice and ceramic particles is produced. Upon sublimation of the ice and sintering of the green ceramic body, a scaffold with unidirectional pores is obtained that can be infiltrated with a polymer or a metal. Control of the freezing conditions, suspension characteristics and additives is paramount to tailor the features of the scaffolds, such as size and morphology of pores, thickness and roughness of ceramic walls, ceramic fraction, etc. [24,29,31,32]. By careful control of the processing parameters, lamellar composites containing up to 45 vol.% of ceramic were first fabricated [24]. These composites showed similarities to nacre but with a lamellar structure with the characteristic surface roughness of the ceramic layers [24]. Shortly afterwards, the same procedure was modified to increase the ceramic fraction up to 80 vol.% and to produce a composite that exhibited a “nacre-like” brick-and-mortar structure resembling many features of the inorganic platelets in the bio-composite (including the presence of ceramic bridges) [6]. Starting from ice-templated structures, both lamellar and brick-and-mortar composites consisting of alumina and polymethyl methacrylate (PMMA) were produced that displayed exceptional toughness and strength. Combining a ceramic, which provides for strength, with a relatively soft polymer acting as a “compliant” or “lubricant” phase led to final materials that exhibited a rising R-curve behavior with fracture toughness up to 300 times higher, in energy terms, than that of the main constituents [6,25]. However, systematic investigations of the effects of structural parameters, such as lamellae thickness, presence of ceramic bridges, ceramic fraction, etc., on the mechanical response of these hybrid composites has to date been largely overlooked. Launey et al. reported that varying the thickness of the ceramic layer in lamellar Al_2O_3-PMMA composites had an almost negligible effect on the flexural strength [25], but their study was focused on a comparison between lamellar and brick-and-mortar composites, rather than the investigation of the relationship between structural features of the composites obtained from freeze-cast structures and their mechanical performance.

Based on observations that the structures obtained by freeze casting can change considerably by varying the processing parameters [29], the objective of the current study was specifically to investigate the influence that these changes can have on the mechanical response of ceramic/polymer lamellar composites. As silicon carbide (SiC) had never been examined in this context, we used freeze casting to fabricate SiC scaffolds with characteristic pores morphologies, either lamellar or dendritic. These scaffolds were infiltrated with PMMA generating composites that vary in ceramic content (40–60 vol.%), lamellae thickness (5–35 μm) and the number of ceramic bridges between the individual lamellae. The mechanical behavior of these composites is described in terms of flexural strength and resistance to failure using micro-notched samples loaded in three-point bending. The results obtained show a clear dependence of the damage tolerance of these materials on the ceramic content of the individual composites and a strong correlation with the structure achieved by varying processing routines.

2. Experimental procedures

2.1. Processing

Porous silicon carbide scaffolds were prepared by freeze casting, following the procedure described in detail in our previous study [29]. We prepared suspensions containing 17–30 vol.% of SiC powders with sintering aids (Al_2O_3 and Y_2O_3) dispersed in deionized water, and added 5 wt.% polyethylene glycol (PEG) as a binder. The suspensions were electrostatically stabilized by adding ammonium hydroxide (NH_4OH) to change the pH to 10 and by ball milling for 40 h. Ice-templated scaffolds were produced by freezing the SiC suspensions at cooling rates between −1 and −15 °C min^{-1}. After water sublimation, the scaffolds were first treated in air at 450 °C for 4 h and then sintered in inert atmosphere at 1900 °C for 30 min. Details on the effects of the processing parameters on the ceramic fraction and the architecture of the scaffolds are reported elsewhere [29]. Based on that study, we selected a combination of parameters to produce scaffolds with three different ceramic contents: 40, 50 and 60 vol.%. For samples containing 50 vol.% ceramic, we produced scaffolds with either lamellar or dendritic morphology.

The SiC scaffolds were infiltrated with PMMA in order to fabricate composites and assess the influence of the different architectures on the mechanical properties. The polymer infiltration was carried out in two steps, preceded by grafting of the ceramic surface. For this purpose, the ceramic scaffolds were immersed in 50 vol.% solution of 3-(trimethoxysilyl) propyl methacrylate (γ-MPS) in acetone for 12 h. After drying, the grafted scaffolds were immersed in a solution of methyl methacrylate (MMA) in toluene (toluene:MMA 2:1 by weight) for 2 h at 70 °C to perform free

---

[2] Expressing the toughness in energy terms, i.e., in terms of the critical strain-energy release rate, G_{Ic}, the toughness of nacre is some three orders of magnitude higher than the toughness of its constituent phases.

radical polymerization initiated by 2,2′-azobisisobutyronitrile (AIBN, 1 wt.% respect to MMA). In the last step, free radical polymerization was carried out without the solvent, in bulk (0.5 wt.% AIBN, 70 °C for 12 h). Further details of the polymerization procedure are reported elsewhere [25]. Using this procedure, the pores of the SiC scaffolds were completely filled with PMMA.

The resulting SiC/PMMA composites consisted of 40, 50 and 60 vol.% of ceramic, depending on the processing parameters used; hereafter, these samples are referred to as SiC40/PMMA, SiC50/PMMA and SiC60/PMMA, respectively. Samples SiC50/PMMA, containing an equal fraction of the two constituents, were also produced using scaffolds with the same ceramic content, i.e., 50 vol.%, but varying morphologies and ceramic wall thicknesses.

All microstructures were examined using a Hitachi S-4300SE/N (Hitachi America, Pleasanton, CA, USA) scanning electron microscope (SEM) and image analyses were carried out to quantify the ceramic fraction, the thickness of ceramic and polymer layers and the occurrence and frequency of bridges connecting the ceramic lamellae.

The morphologies of the composites were further described using the dimensionless parameter m, which we introduced in a previous study [29] and is defined as $m = (1/\rho_b)/\lambda^2$, where ρ_b is the bridge density (number of bridges between adjacent lamellae per unit area) and λ the lamellae wavelength. We have shown that, by comparing the bridge spacing with the lamellae wavelength, the parameter m can fully describe the morphology of freeze cast scaffolds. It is used here to distinguish between lamellar ($m > 5$) and dendritic ($1 < m < 5$) composites structures.

2.2. Mechanical properties

To evaluate the mechanical behavior of the processed materials, beams for flexural strength tests and single edge-notched bend, SE(B), fracture toughness tests were cut out of the polymer infiltrated scaffolds using a water-cooled low speed saw. Beams for strength tests were made with different cross sections of roughly $(1.5 \times 1.5)\,\mathrm{mm}^2$, $(2 \times 2)\,\mathrm{mm}^2$ and $(3 \times 1.5)\,\mathrm{mm}^2$ and lengths, L between 10 mm and 20 mm, depending on the dimension of the initial infiltrated scaffolds, and the length being well above 4 times the sample width, W, to exclude any effect of shear between the pins; the obtained strength data did not show any significant variation resulting from the different sample sizes. All surfaces were gradually ground and polished to a 1 μm finish and tests were carried out at a displacement rate of 1 μm/s using loading spans between 6 mm and 18 mm on an Instron 5944 electromechanical testing system (Instron Corporation, Norwood, MA, USA). In total, 42 ($N = 42$) samples, at least 3 per ceramic content and processing condition, were tested and evaluated in general accordance with ASTM standard D790 [33].

The beams for SE(B) fracture toughness tests were made with a width, W and a thickness, B of roughly 3 mm and 1.5 mm, respectively, and were tested using a loading span of 12 mm in general accordance with ASTM standard E1820 [34]. (For these tests samples with a cross-sectional area smaller than 3 × 1 mm were excluded as they often do not permit measurement of enough stable crack extension prior to catastrophic failure.) Prior to testing, samples were polished using the same procedure used for the strength beams but were additionally notched with a diamond blade. These notches were then sharpened using a micro-notching technique involving polishing the notch root using a razor blade immersed in 1-μm diamond paste to a final notch root radius between 5 and 20 μm and a crack length, a, to width ratio, a/W, of ~0.5. At least 3 samples per ceramic content and processing condition, 23 ($N = 23$) samples in total, were tested *in situ* in the SEM using a Deben MicroTest 2kN (Deben, UK) bending stage; this permitted the measurement of the R-curve with real-time observations of crack propagation on the surface of the sample during step-wise loading at a displacement rate of 0.55 μm/s. Samples were tested to crack extensions, Δa, well above 0.4 mm, the maximum crack extension capacity for the size of sample used given by the ASTM standard for plane strain J_{Ic} fracture toughness measurement [34] (i.e., $\Delta a_{\max} = 0.25\, b_0$, where b_0 is the initial uncracked ligament width).

To capture both the elastic and plastic contributions from deformation and crack growth to the toughness of the material, nonlinear elastic fracture mechanics analysis was used to determine J-based crack-resistance curves, i.e., J_R as a function of crack extension, Δa. Specifically, the J-integral at each measured crack length, a, was calculated from $J = 1.9A_{\mathrm{tot}}/Bb$, where A_{tot} is the total area under the load-line displacement curve, including both the elastic (often expressed as K_{Ic}^2/E', where $E' = E$, Young's modulus in plane stress and $E/(1-\nu^2)$ in plane strain, where ν is Poisson's ratio) and plastic contributions to the energy, and b is the uncracked ligament width (i.e., $b = W - a$) [34].

Fracture toughness values, expressed in terms of stress intensities, K, were calculated using the standard mode I J–K equivalence relationship, $K_J = (J\,E')^{0.5}$, where J is the J-based fracture toughness. Values for E were estimated using the rule-of-mixtures at 93 GPa for SiC40/PMMA composites, 116 GPa for SiC50/PMMA composites and 139 GPa for the SiC60/PMMA composites, with $\nu = 0.3$ for all composites.[3]

In addition to assuring that valid J-dominant crack-tip fields and plane-strain conditions were maintained, R-curve determination was limited to small-scale bridging conditions, where the size of the zone of crack bridges behind the crack tip remained small compared to the in-plane test specimen dimensions. Where large-scale bridging in evidence, the R-curve shape tends to display a concave-up appearance. In our work, all R-curve data are shown with dashed lines indicating where the results become invalid. As such, all quoted valid toughness values were measured before this condition was reached, as large-scale bridging can result in erroneously high, specimen size-dependent, toughness values [6]. Certain previous results in the literature on such hybrid materials [9] appear to display such errors.

3. Results

3.1. Microstructure

Processing parameters, such as suspension solid content and cooling rate during freezing, invariably affect both ceramic fraction and morphology of the freeze-cast scaffolds. Simultaneously varying these parameters enabled us to tune the scaffolds architecture and the ceramic content, obtaining different morphologies and a wide range of lamella thickness.

Fig. 1 shows two examples of microstructure for SiC/PMMA composites, namely (a) SiC40/PMMA and (b) SiC60/PMMA, containing respectively 40 and 60 vol.% of SiC. SiC40/PMMA samples were obtained by freezing suspensions with 17 vol.% ceramic powder at $-1\,^{\circ}\mathrm{C\,min^{-1}}$. For SiC60/PMMA samples, we used a suspension with 25 vol.% solid content and a freezing rate of $-15\,^{\circ}\mathrm{C\,min^{-1}}$. The freeze-cast scaffolds were then sintered and used to prepare composite materials following the procedures described above. The mean thickness of the ceramic lamellae was ~7.5 and ~9 μm, respectively, for samples of SiC40/PMMA and

---

[3] Despite the very limited impact of uncertainties in E on the J–K equivalence [6], influences of structural variations of our SiC/PMMA composites on their mechanical properties are assessed principally in terms of the material's J-based resistance curve response (without the use of E); however, for comparison to other materials, we do back-calculate and plot the R-curves in terms of K_J-values at the end of this paper.

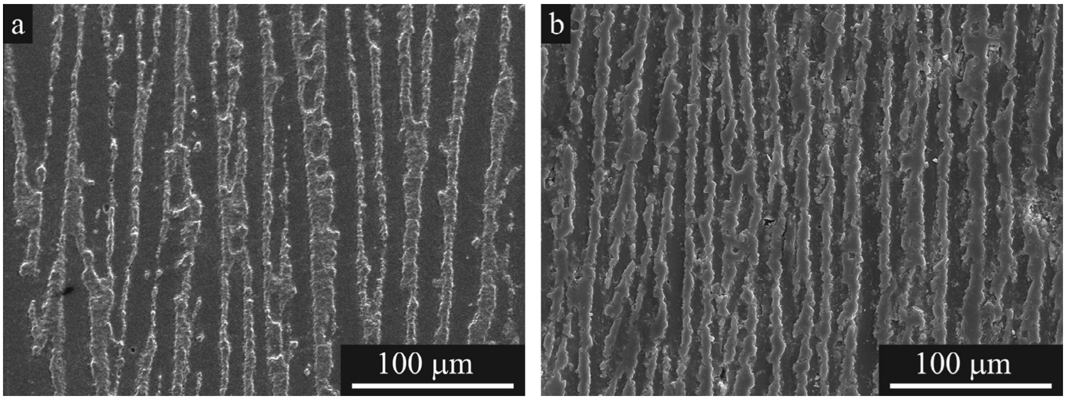

Fig. 1. SEM micrographs of samples of (a) SiC40/PMMA, containing 40 vol.% of SiC and 60 vol.% of PMMA, and (b) SiC60/PMMA, containing 60 vol.% of SiC and 40 vol.% of PMMA. The bright phase is SiC; the dark phase is PMMA. The composites were fabricated by polymer infiltration of freeze-cast scaffolds obtained under different processing conditions. (a) Scaffolds for SiC40/PMMA samples were prepared from a ceramic suspension at 17 vol.% solid content, frozen at $-1\ ^\circ\mathrm{C\ min^{-1}}$; the final SiC40/PMMA composites had a lamellar morphology ($m \sim 22$) and ceramic layers of ~7.5 μm. (b) The starting suspension for SiC60/PMMA samples contained 25 vol.% solid content and was frozen at $-15\ ^\circ\mathrm{C\ min^{-1}}$; these composites had a lamellar morphology with more connected ceramic lamellae ($m \sim 10$) of ~9 μm.

SiC60/PMMA. The scaffolds were fully infiltrated by PMMA. Both samples exhibited a lamellar morphology, however, SiC40/PMMA had a lower density of bridges than SiC60/PMMA. The morphological parameter m was ~22 for SiC40/PMMA, and ~10 for SiC60/PMMA.

Composites showing different lamellae thicknesses and morphologies were produced with a ceramic fraction of 50 vol.% and are referred to as SiC50/PMMA-a to d. The scaffolds used to produce these samples were obtained by varying both solid content of the starting suspensions and freezing conditions. We prepared four sub-series of samples SiC50/PMMA, the lamellae thickness ranging from 5 to 35 μm (Fig. 2). Scaffolds with lamellae thickness of 35 μm were produced by freezing suspensions with 30 vol.% solid content at $-1\ ^\circ\mathrm{C\ min^{-1}}$; these scaffolds were successfully infiltrated to produce composites with lamellar morphology ($m \sim 17$), referred to as SiC50/PMMA-a (Fig. 2a). As reported previously [29], under certain freezing conditions and suspension solid contents, the ice crystallizes in a dendritic pattern rather than lamellar, leaving tortuous pores in the ceramic scaffolds; the faster the cooling rate the smaller and more tortuous the ice crystals and hence the pore structure. Suspensions with 25 vol.% solid content were frozen at −5 and $-10\ ^\circ\mathrm{C\ min^{-1}}$ yielding scaffolds with a more dendritic morphology. The composites made with these scaffolds, referred to as SiC50/PMMA-b and SiC50/PMMA-c, are shown, respectively, in Fig. 2b and c. SiC50/PMMA-b samples (Fig. 2b) have a lamellae thickness of ~12 μm and few bridges connecting them, while Si50/PMMA-c samples (Fig. 2c), made with scaffolds frozen at a faster cooling rate, have finer ceramic lamellae of ~7 μm and show a significant presence of ceramic bridges. These differences in structural morphology can again be represented by the morphological parameter: $m \sim 8.5$ for SiC50/PMMA-b composites indicating a lamellar/*quasi*-dendritic morphology, while a value of $m \sim 4.5$ for SiC50/PMMA-c samples is characteristic of a dendritic structure.

Composites with even finer lamellae of ~5 μm (Fig. 2d), referred to as SiC50/PMMA-d, were made using scaffolds prepared from a suspension with 17 vol.% solid content, frozen at $-10\ ^\circ\mathrm{C\ min^{-1}}$. These samples showed the largest parameter $m \sim 27$, despite a slightly higher density of bridges when compared to the other lamellar composites that had $m > 5$. However, the bridge spacing in SiC50/PMMA-d was much larger than the lamellae wavelength, giving the structure a rather lamellar character.

Comparing samples with different volume fractions, SiC40/PMMA and SiC50/PMMA-a composites show a similar lamellar morphology despite their very different lamellae thickness. The SiC50/PMMA-b morphology, however, is closer to that of the SiC60/PMMA samples.

3.2. Mechanical behavior: strength

Three-point bending tests were performed to determine the flexural strength of the various processed materials (Fig. 3). Fig. 3a compares the average strength levels of samples with the same ceramic content; SiC40/PMMA shows a flexural strength of 91.3 ± 3.6 MPa, the average values of all SiC50/PMMA samples are 127.7 ± 23.5 MPa, and the SiC60/PMMA samples have a strength of 164.5 ± 19.4 MPa. This trend clearly follows the expected increase of strength with increasing ceramic content. The effect of the microstructure, in particular morphology and lamella thickness, on the flexural strength can be seen in Fig. 3b where the average strength values of the four sub-classes of the SiC50/PMMA materials are indicated. The strength of these samples varies significantly between 110 and 150 MPa according to the morphology of the ceramic scaffolds. SiC50/PMMA-c, a composite with a dendritic morphology and ~7 μm thick ceramic walls connected by many bridges, showed the highest strength of 148.8 ± 18.5 MPa. Despite their very different morphology, the SiC50/PMMA-a and SiC50/PMMA-b composites had very similar strengths of 126.6 ± 9.7 MPa and of 124.7 ± 26.0 MPa, respectively. In particular, SiC50/PMMA-a samples had a coarse lamellar morphology, the thickness of the ceramic layers being up to 35 μm (Fig. 2a), while SiC50/PMMA-b samples had finer but interconnected ceramic walls with thickness of ~12 μm (Fig. 2b). SiC50/PMMA-d samples showed the lowest strength with 108.4 ± 6.5 MPa. This material has a lamellar morphology with fine ceramic walls (~5 μm) and few ceramic bridges connecting them (Fig. 2d).

3.3. Mechanical behavior: fracture toughness

To characterize the composites in terms of their fracture toughness, J_R-curve measurements were performed to evaluate their resistance to failure. The R-curves are shown in Fig. 4 for samples of different ceramic content, i.e., 40, 50 and 60 vol.% (Fig. 4a) and for samples of same ceramic content (50 vol.%) but different morphology in Fig. 4b.

Similar to the variation in strength (Fig. 3a), the fracture toughness of the composites strongly correlates with the content of ceramic revealing a reduced fracture resistance (in energy terms) with higher ceramic fraction (Fig. 4a). All tested materials show an

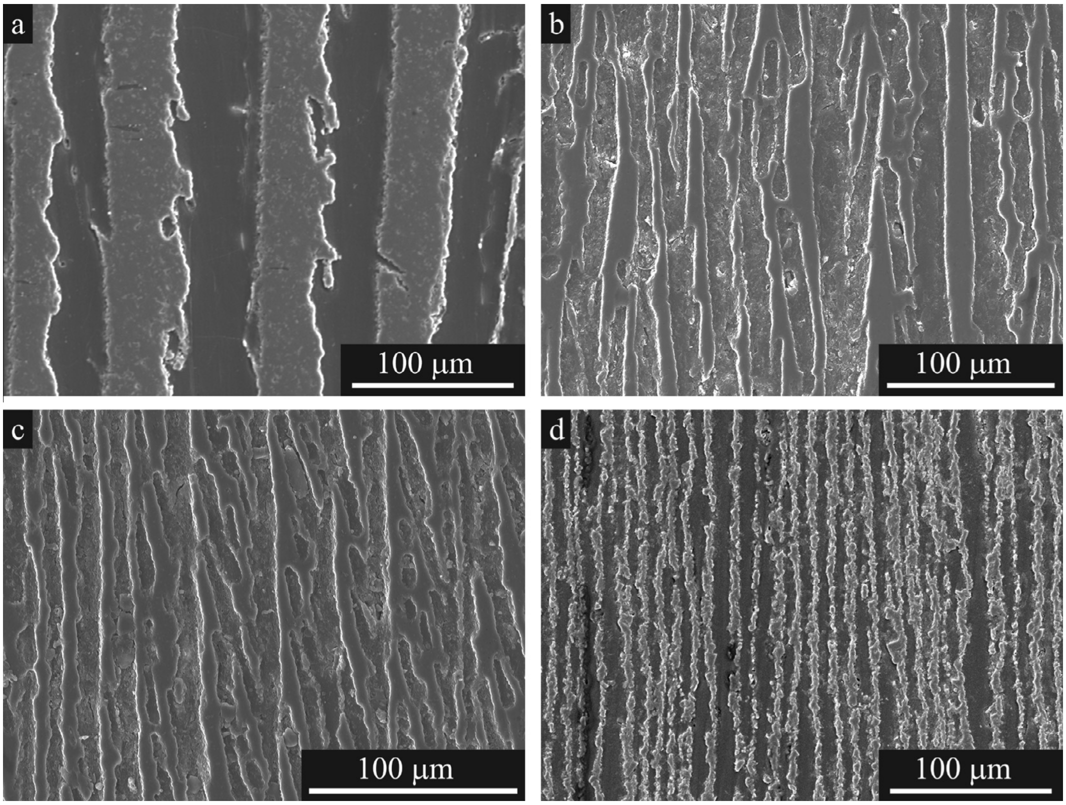

Fig. 2. SEM micrographs of SiC50/PMMA samples containing 50 vol.% of SiC and 50 vol.% PMMA. Combining proper freezing conditions and contents of the ceramic suspensions, the composite architectures could be varied. Scaffolds for (a) SiC50/PMMA-a samples were prepared with ceramic suspensions at 30 vol.% solid content, frozen at −1 °C min^{-1}, and exhibit a lamellar morphology ($m \sim 17$) with ceramic layers (bright phase) of ~35 μm. Scaffolds for (b) SiC50/PMMA-b and (c) SiC50/PMMA-c samples were prepared from suspensions at 25 vol.% solid content, frozen at −5 and −10 °C min^{-1}, respectively. (b) SiC50/PMMA-b composites have a morphology intermediate between lamellar and dendritic ($m \sim 8.5$), with ceramic lamellae of ~12 μm. (c) SiC50/PMMA-c samples exhibit a finer dendritic structure ($m \sim 4.5$), with more bridges connecting ceramic lamellae of ~9 μm. (d) SiC50/PMMA-d samples were prepared starting from suspensions with 17 vol.% solid content, frozen at −10 °C min^{-1}; these conditions led to samples showing a higher density of bridges than the other lamellar composites and very thin ceramic lamellae of 5 μm ($m \sim 27$). (The ceramic lamellae in each image are the somewhat lighter phase.)

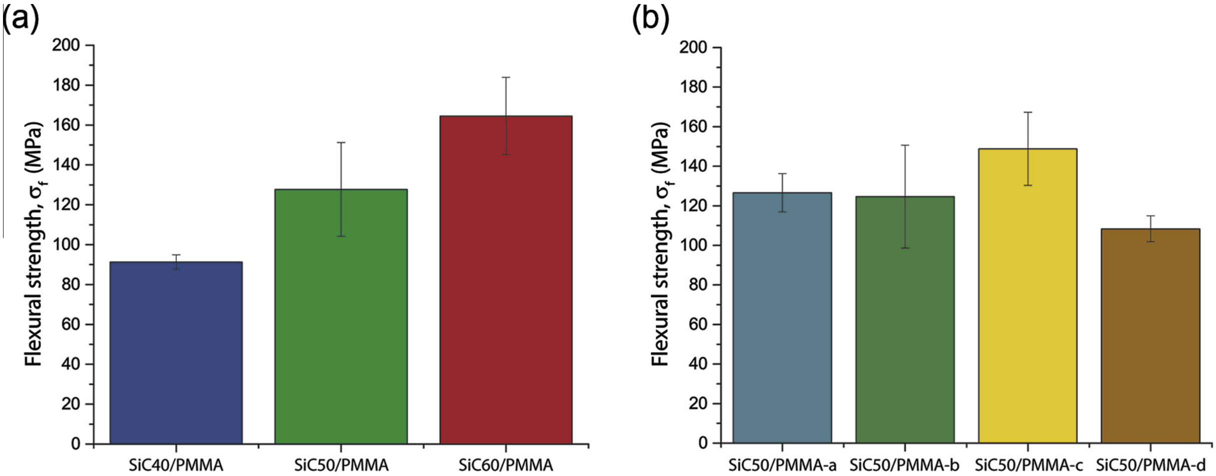

Fig. 3. Average values of flexural strength for SiC/PMMA composites. (a) The strength of the composites shows a significant increase with increasing ceramic content resulting in 91.3 ± 3.6 MPa for the SiC40/PMMA materials (40 vol.% ceramic), 127.7 ± 23.5 MPa for the SiC50/PMMA samples (50 vol.% ceramic), and 164.5 ± 19.4 MPa for the SiC60/PMMA (60 vol.% ceramic). (b) The different morphologies and wall thicknesses show a strong influence on the flexural strength of the composites at the same ceramic fraction of 50 vol.% (SiC50/PMMA). SiC50/PMMA-c samples have the highest strength of 148.8 ± 18.5 MPa due to their highly dendritic morphology ($m \sim 4.5$) and relatively thin lamellae (~7 μm), SiC50/PMMA-a samples with 126.6 ± 9.7 MPa and SiC50/PMMA-b samples with 124.7 ± 26.0 MPa are very similar in strength despite their very different structure. The SiC50/PMMA-a material has a lamellar morphology ($m \sim 17$) with very thick ceramic layers (~35 μm), while SiC50/PMMA-b has thinner lamellae (~12 μm) and a *quasi*-dendritic morphology ($m \sim 8.5$), although with less bridges than SiC50/PMMA-c. SiC50/PMMA-d samples, with thin lamellae (5 μm) and few bridges ($m \sim 27$), exhibit the lowest strength levels with 108.4 ± 6.5 MPa.

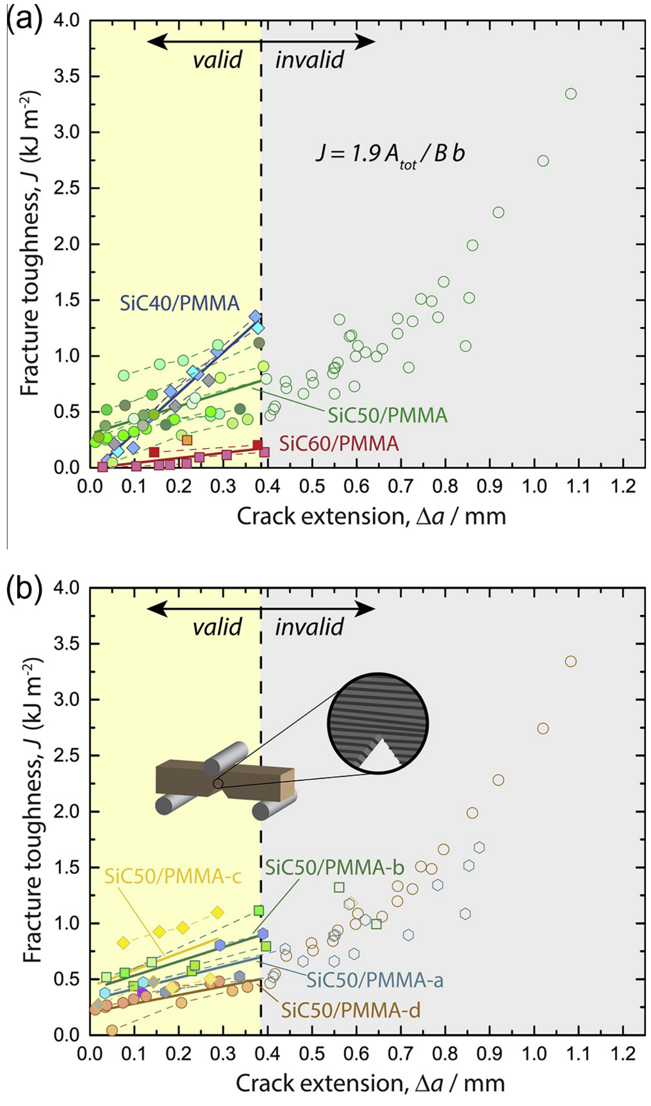

Fig. 4. Crack-resistance curves (R-curves) in terms of J as a function of crack extension, Δa, for (a) the three classes of composites SiC40/PMMA, SiC50/PMMA and SiC60/PMMA, and (b) the four sub-classes of SiC50/PMMA samples having the same ceramic fraction of 50 vol.% but different morphology and lamellae thicknesses. Resistance to crack growth is clearly dependent on the volume fraction of the two constituents, being proportional to the amount of polymer in the composites (a). However, when samples with same ceramic content are compared, the influence of the morphology emerges (b): SiC50/PMMA-c samples, in which ceramic walls of ~7 μm significantly interconnected ($m \sim 4.5$), and SiC50/PMMA-b, with thinner ceramic layers of ~12 μm and fewer bridges connecting them ($m \sim 8.5$), exhibit the highest R-curves; the toughness decreases for SiC50/PMMA-a and SiC50/PMMA-d composites with the lamellar morphology, regardless the lamellae thickness. In these samples, the ASTM standard [34] permits a maximum Δa of ~0.4 mm; crack-growth data above this limit are strictly “invalid”.

increasing fracture resistance with crack extension with fracture toughness J values of ~1.25 kJ m^{-2} for SiC40/PMMA, ~0.75 kJ m^{-2} for SiC50/PMMA and ~0.25 kJ m^{-2} for SiC60/PMMA, all measured at $\Delta a \sim 0.4$ mm. In terms of stress intensities, these J-based toughness values are equivalent to K-based values in the range of ~6 to 12 MPa m$^{0.5}$, for data that are strictly “valid” in terms of ASTM Standard 1820 [34]; crack-growth toughness values that exceed the crack extension limit of ~0.4 mm are considerably higher, ranging from ~8 to 19 MPa m$^{0.5}$.

While the crack growth of the two materials with the higher ceramic content seems comparable, SiC40/PMMA samples show a much steeper slope for crack growth but a lower crack-initiation toughness than the SiC50/PMMA samples. Samples with 50 vol.% SiC but different morphologies show significant differences in their crack-growth behavior, as shown in Fig. 4b. SiC50/PMMA-b samples, which had thin ceramic layers of ~12 μm and an incipient dendritic morphology, showed a fracture resistance up to at least $J \sim 0.85$ kJ m^{-2} at crack extensions of roughly 0.4 mm. SiC50/PMMA-c, a composite with thinner ceramic walls (~7 μm) and a pronounced dendritic morphology, showed a similar resistance to failure with $J \sim 0.85$ kJ m^{-2} at crack extensions of roughly 0.3 mm. In comparison, a SiC50/PMMA-a sample, characterized by a coarse lamellar morphology, reached a fracture resistance of $J \sim 0.68$ kJ m^{-2}; SiC50/PMMA-d samples, having the finer lamellar morphology, displayed the most brittle behavior with a fracture resistance of ~0.5 kJ m^{-2}.

3.4. Crack-growth observations

With *in situ* R-curve measurements in the scanning electron microscope, the evolution of damage, crack–path interactions with microstructure and the resulting toughening mechanisms could all be observed during three-point bending loading of the SE(B) specimens.

After crack initiation at the root of the micro-notch, crack extension occurred in a stable, subcritical manner, nominally in a direction perpendicular to the maximum tensile stress; an example for such crack growth, observed in lamellar SiC50/PMMA-a composites, is shown in Fig. 5a. The damage resulted principally in microcracking of SiC lamellae ahead of the propagating crack (Fig. 5b) and inelastic deformation of the PMMA layers undergoing extensive tearing and stretching, thereby acting as uncracked ligament bridges (a potent form of extrinsic toughening) prior to failure (Fig. 5c). Additionally, “pull out” of ceramic lamellae, with significant shear deformation within the polymer layers, was observed (Fig. 5d).

Other forms of damage accumulating during crack propagation in composites with 40 and 60 vol.% SiC are shown in Fig. 6a and b, respectively. Here in both materials, cracking of the ceramic lamellae ahead of the propagating crack was observed as an initial failure mechanism. In the SiC40/PMMA composite, the polymer layers failed after extensive inelastic deformation through the nucleation and coalescence of microvoids (Fig. 6a). In SiC60/PMMA, where the polymer layers were thinner, the PMMA showed extensive shear deformation before failure (Fig. 6b).

Fig. 7 shows a typical example of a SiC/PMMA fracture surface after testing. We observed brittle intergranular fracture of the ceramic walls and extensive plastic deformation of the polymer layers, which exhibited clear tearing and stretching (Fig. 7). Moreover, the examination of the fracture surfaces confirmed the effectiveness of the grafting of the ceramic surface, which improved the interface between SiC and PMMA: despite the extensive plastic flow of the polymer, interfacial debonding rarely occurred (Fig. 7).

4. Discussion

4.1. Microstructure

Freeze casting provides a unique process to tune the architecture of ceramic scaffolds that, when infiltrated with a second (compliant) phase, e.g., a polymer or metal, can be used to produce nature-inspired composites with uncommon combinations of mechanical properties. The porosity that is being filled with a compliant phase is the exact replica of the ice developed during freezing. As the ice morphology depends on the freezing procedure and the suspension characteristics, processing parameters such as cooling rate and solid content in the ceramic slurry can be readily

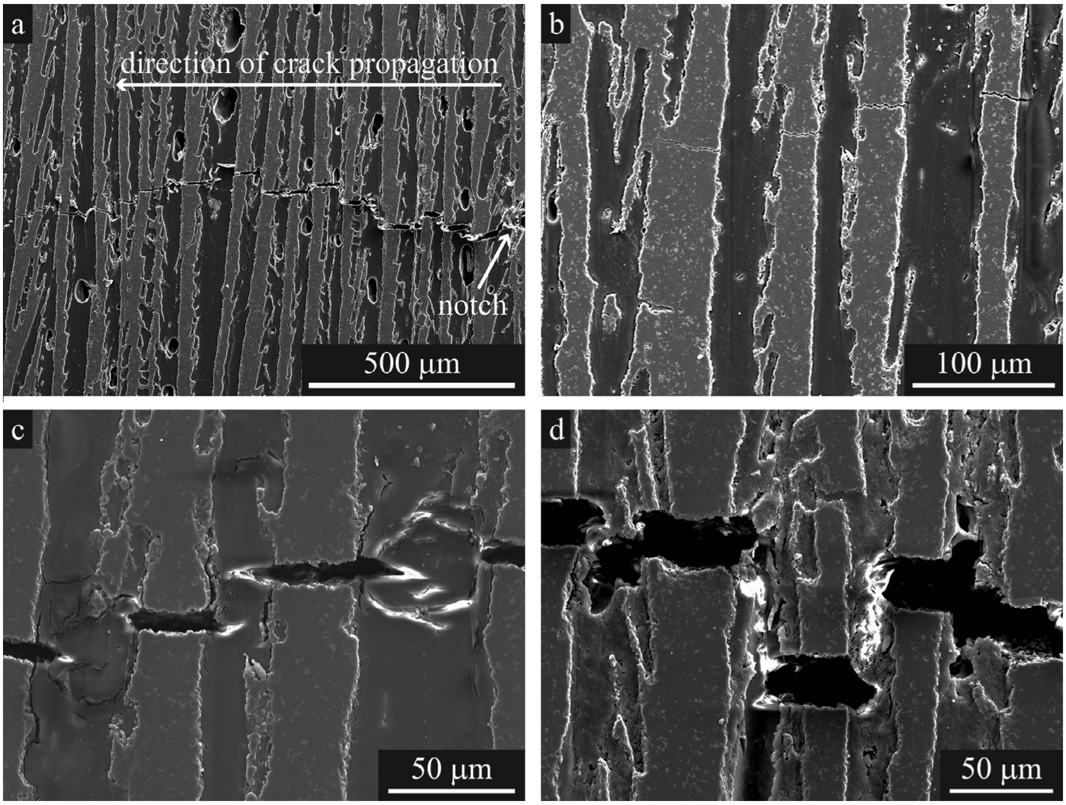

Fig. 5. SEM micrographs taken during *in situ* R-curve measurements of the toughness of lamellar SiC50/PMMA-a composites. (a) The main crack propagated along a coplanar path from the sharpened notch (right-hand side), under the tensile driving force ahead of the crack tip, generated by mode I loading (crack propagation is nominally from the right to left). (b) Initially, distributed damage in the form of cracks within the ceramic lamellae and uncracked-ligament bridging is observed, then (c) the polymer layers undergo extensive plastic deformation. (d) "Pull out" of ceramic lamellae, causing significant shear deformation within the polymer, was also observed.

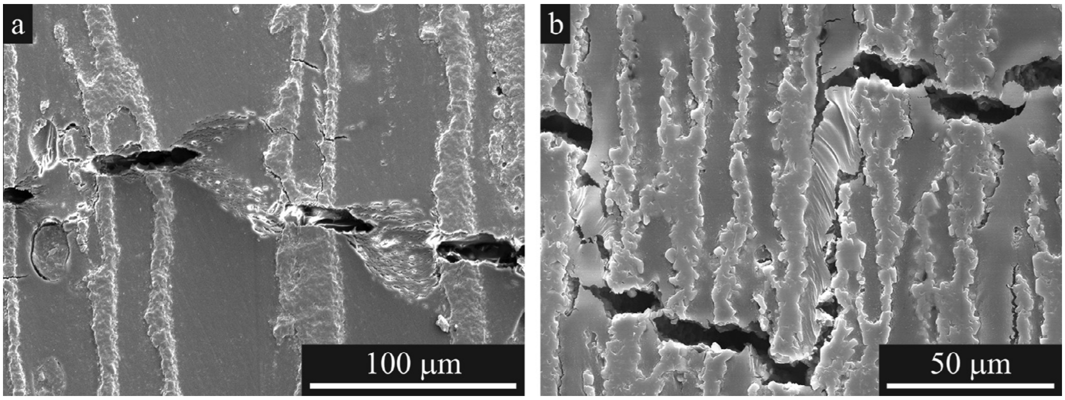

Fig. 6. SEM micrographs taken during *in situ* R-curve measurements of the toughness of SiC/PMMA composites. (a) In SiC40/PMMA samples, we observed extensive plastic deformation within the polymer, followed by nucleation, growth and coalescence of microvoids before macroscopic crack advance. (b) In SiC60/PMMA samples the polymer layers often exhibited considerable shear deformation leading to polymer/ceramic interface failure.

modified to optimize the scaffold morphology and so achieve the desired properties, specifically that of damage tolerance, in the hybrid structures.

The solid content in the suspension affects primarily the ceramic fraction of the final scaffold, but has effects also on the ceramic lamellae thickness and morphology of the pores [29]. Generally, an increase in the suspension solid content yields a higher ceramic fraction in freeze-cast scaffolds. This can be appreciated by comparing samples from suspensions with different solid content frozen under similar conditions. For instance, the SiC40/PMMA (Fig. 1a) and SiC50/PMMA-a (Fig. 2a) composites were produced from suspensions containing a solid content of 17 and 30 vol.%, respectively, and frozen at $-1\,^{\circ}\mathrm{C\,min^{-1}}$. Both samples show a lamellar morphology which is a consequence of the very slow freezing conditions. SiC50/PMMA-a, however, contains a larger ceramic fraction, 50 vol.%, than SiC40/PMMA with 40 vol.%. The thickness of the ceramic lamellae is also affected by the solid content in the suspension: an increasing concentration of the slurry results in thicker lamellae, when other processing parameters are kept constant. This can be seen for example in Fig. 2a, where SiC50/PMMA-a has thicker ceramic layers (~35 µm) than SiC40/PMMA (~7.5 µm), shown in Fig. 1a.

The cooling rate affects both the lamella thickness and the morphology. Faster freezing causes a refinement of the structure in

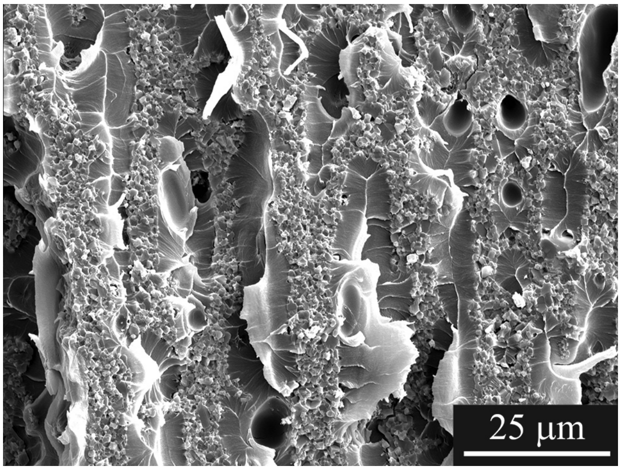

Fig. 7. SEM micrograph of a fracture surface examined after R-curve testing of a SiC50/PMMA-c, showing plastic deformation and extensive tearing of the PMMA layers and brittle fracture of SiC lamellae.

terms of lamellae thickness, but can also change the ice morphology from large lamellar to small dendritic crystals. Consequently, the pore morphology changes, the number of bridges connecting the ceramic lamellae increases, and the densification of the scaffold during sintering is promoted, resulting in a higher ceramic fraction [29]. This becomes evident when comparing samples made from SiC40/PMMA (Fig. 1a) and SiC50/PMMA-d (Fig. 2d), which were prepared from suspensions with 17 vol.% of solid content, but frozen at −1 and −10 °C min^{-1} respectively. SiC50/PMMA-d exhibits finer lamellae (~5 μm) and a higher density of bridges than SiC40/PMMA (~7.5 μm) and higher ceramic fraction, as it was frozen faster.

By carefully selecting suspension solid content and cooling rate, we produced scaffolds with very different morphology and lamellae thickness, but same ceramic fraction of 50 vol.%. In particular, the more concentrated slurries (30 vol.% solid content) were frozen at a slow cooling rate of −1 °C min^{-1}, to produce SiC50/PMMA-a samples (Fig. 2a). To obtain composites with same ceramic fraction and a refined morphology, as in SiC50/PMMA-b and c (Fig. 2b and c), suspensions with 25 vol.% solid content were frozen at cooling rates as fast as −5 and −10 °C min^{-1}. These scaffolds showed more bridges connecting the ceramic layers and smaller pores when compared with SiC50/PMMA-a, promoting further densification during sintering. Furthermore, solidification at −10 °C min^{-1} of a suspension with 17 vol.% solid content yielded samples with a ceramic fraction of 50 vol.%, with ceramic lamellae on the order of 5 μm thick, and the presence of bridges.

4.2. Mechanical behavior

Strength and toughness testing and *in situ* characterization of crack extension provide crucial information on how changes in the architecture of the SiC/PMMA composites can influence their mechanical performance. A property map based on our findings is shown in Fig. 8 to provide further illustration of this complex relationship. Fracture toughness *vs.* flexural strength values are plotted for each group of composites; schematics of the samples morphology and arrows indicating the direction of increase of the ceramic content, the lamellae thickness, and the density of interlayer bridges are also shown to help visualize further trends in mechanical properties.

While the *strength of the SiC/PMMA composites is directly proportional to their ceramic fraction* (Figs. 3a and 8) over a relatively narrow range of ceramic contents (40–60 vol.%) and for

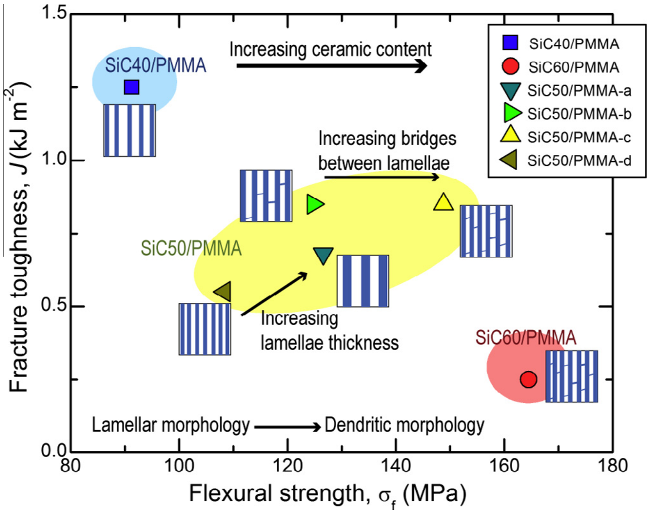

Fig. 8. Property map comparing the mechanical performance of the various SiC/PMMA composites examined in this study (schematics of the architecture of each group of samples are depicted, in which the ceramic is represented in blue and the polymer in white). Both flexural strength and (energy-based) fracture toughness depend on the ceramic content in the composites; specifically, the strength is directly proportional and the toughness inversely proportional to the ceramic fraction in the range 40–60 vol.%. Indeed, SiC40/PMMA composites, with 40 vol.% ceramic, show the lowest strength and the highest toughness, while SiC60/PMMA samples, comprising of 60 vol.% SiC, exhibit the maximum strength and the minimum toughness. Between these two limiting cases, samples with 50 vol.% ceramic display intermediate values of strength and toughness, depending on structural features such as lamellae thickness and morphology. Among the four sub-classes of SiC50/PMMA composites, the group that behaves the worst in terms of both strength and toughness is SiC/PMMA-d, with thin ceramic layers (5 μm) and a lamellar morphology where the bridge spacing is much larger than the lamellae wavelength ($m \sim 27$). However, the mechanical performance can be improved by either increasing the lamellae thickness, as for SiC50/PMMA-a, or modifying the morphology from lamellar to dendritic and thus enhancing the presence of bridges that connect the ceramic layers, as in SiC50/PMMA-b and SiC50/PMMA-c. This latter approach which involves a marked change in morphology appears to be particularly effective. In SiC50/PMMA-c samples, for example, which are characterized by a dendritic morphology ($m \sim 4.5$), the significant presence of ceramic bridges yields a strengthening effect without loss in toughness.

a given morphology, this study shows that the strength also varies significantly with scaffold morphology (lamellar *vs.* dendritic), lamellae thickness and the presence of bridges connecting the ceramic layers (Figs. 3b and 8), although the correlation with strength of the latter variable at fixed ceramic content is quite complex.

At a ceramic fraction of 50 vol.%, SiC50/PMMA-c samples with a dendritic morphology ($m \sim 4.5$), with interconnected lamellae of ~7 μm, exhibited the highest strength (148.8 ± 18.5 MPa); SiC50/PMMA-a, with lamellar morphology and thicker ceramic layers of ~35 μm ($m \sim 17$), and SiC50/PMMA-b, characterized by finer lamellae of ~12 μm and a morphology intermediate between lamellar and dendritic ($m \sim 8.5$), had similar strength values (~125 MPa) despite their very different microstructure. SiC50/PMMA-d composites, which exhibited the lowest strength (108.4 ± 6.5 MPa), had very fine lamellae of ~5 μm. For a class of composites with same ceramic fraction such as SiC50/PMMA samples, the strength seems correlated with the morphological parameter m: the smaller is m, the higher is the strength. These results suggest that the main contribution to the strength of these composites is the presence of the bridges connecting the ceramic layers which, akin to nacre [12], prevent the delamination of the ceramic platelets.

In terms of crack-growth toughness, (similar to the strength properties) there was a clear trend with respect to the fraction of the ceramic in the SiC/PMMA composites, *specifically that the toughness (in energy terms) decreased when the ceramic content increased* (Figs. 4a and 8). Also (similar to the strength properties), the toughness varied with scaffold morphology, lamellae thickness and the presence of interlayer bridges (Fig. 8), although again the trends were not always readily apparent. SiC40/PMMA samples exhibit the highest toughness as they contain the largest fraction of polymer that allows extensive inelastic deformation. Conversely, SiC60/PMMA samples show the lowest toughness and the highest strength, having the largest fraction of ceramic that is the load-bearing but brittle phase. While this trend in toughness with volume fraction of ceramic is not very surprising, the contributions of the structural features of composites with the same volume fraction but different morphologies and lamella thickness to the material's fracture resistance are not as straightforward. Our results show that composites with a small parameter m, indicative of *quasi*-dendritic or dendritic structure ($m \sim 8.5$ for SiC50/PMMA-b and $m \sim 4.5$ for SiC50/PMMA-c, shown in Fig. 2b and c, respectively) have a much higher toughness than lamellar ones characterized by higher m ($m \sim 17$ for SiC50/PMMA-a and $m \sim 27$ for SiC50/PMMA-d in Fig. 2a and d). This suggests that ceramic bridges between lamellae, and interface roughness in general, represent factors that can enhance both strength and toughness concomitantly (Fig. 8), which is likely achieved through a controlled sliding of the individual ceramic layers. This effect of ceramic bridges of micrometer and sub-micrometer dimensions is clear, and is known to be a potent mechanism of toughening through efficient energy dissipation, both in natural [12] and synthetic nacre-inspired composites [6,25]. With respect to resistance to crack propagation, all composites exhibited subcritical crack growth with a rising R-curve behavior, which are indicative of extrinsic toughening. Multiple toughening mechanisms were identified in all the composite structures, and included the pull-out of ceramic lamellae, uncracked-ligament bridging, crack deflection, inelastic deformation of ductile polymeric layers, and the fracture of ceramic bridges; these mechanisms are all active to varying degrees in natural nacre [10–13]. Fig. 5 shows clear evidence of premature fracture of the ceramic layers with cracks then arrested in the polymeric interlayers; subsequent loading then results in classic crack bridging with ceramic lamellae pull-out, which clearly are prime mechanisms of R-curve toughening in these materials. Similarly the extensive plastic deformation in the polymeric layers, coupled with void nucleation and growth, shown in Fig. 6, can also lead to considerable shear deformation in the more compliant phase, which results in elastic bridging and severely deflected cracks, all of which contribute to the extrinsic toughening.

In traditional composites such as continuous-fibers-reinforced ceramic composites, the increase in toughness is often associated with a decrease in strength. These composites are toughened through crack bridging by the reinforcing fibers that span the crack wake after the matrix fails. For this mechanism to be effective, the matrix-fiber bonding must be weak, often causing a loss in through-thickness strength [3]. Similarly, conventional layered composites toughened by crack deflection need weak interfaces that can negatively affect strength.

In contrast, our polymer-infiltrated ceramic scaffolds exhibit some enhancement in both strength and toughness when dendritic morphologies are developed during freeze casting, although our measured strength levels are not high; strength levels are comparable to freeze-cast lamellar alumina/PMMA composites [6,8,25] and roughly 20% lower than continuous SiC-fiber reinforced SiC composites). Here, compared to the latter SiC_f–SiC_m material, the improvement in toughness is not necessarily achieved by interface weakening that also can lower the strength of the structure, but rather through the fracture of ceramic bridges between lamellae, which generates a strengthening effect and contributes to controlled lamellae sliding. For samples without dendrites that have a lamellar morphology and poorly connected ceramic layers, we still observe the occurrence of multiple toughening mechanisms, particularly the inelastic deformation of ductile layers. However, where these materials contain 50 vol.% of the polymer that is not a load-bearing phase, the absence of ceramic bridges in the non-dendritic structures means that no mechanism exists to limit lamellae sliding; the result is far more effective toughening in the dendritic, as compared to the lamellar, composites.

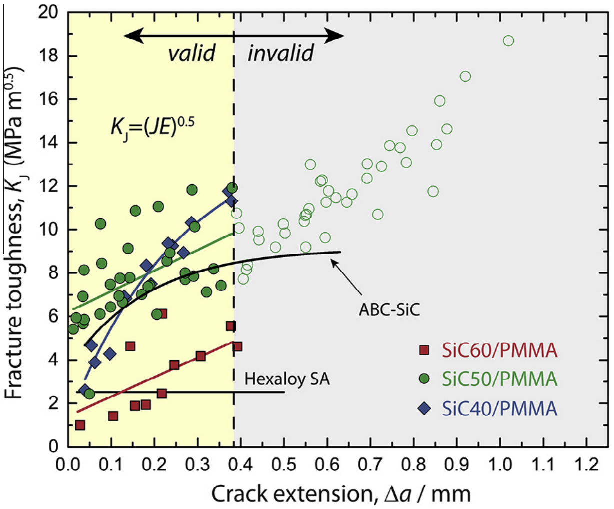

Fig. 9. Fracture toughness crack-resistance curves, presented in stress intensity terms, showing a comparison of the current SiC/PMMA hybrid materials with monolithic SiC ceramics [35,36], both commercial SiC (Hexoloy SA) and *in situ* toughened ABC-SiC. Note that the SiC/PMMA hybrid materials can display superior R-curve toughnesses, with ASTM "valid" values up to 12 MPa m$^{0.5}$. However, measurements for the 40 vol.% SiC/PMMA material suggest crack-growth toughnesses as high as 14 MPa m$^{0.5}$ and for the 50 vol.% SiC/PMMA material as high as 19 MPa m$^{0.5}$, although these values are "invalid" as they occur for crack extensions that exceed $\Delta a \sim 0.4$ mm, the maximum extent of crack growth permitted by the ASTM Standard for the size of our specimens. (Crack-growth data above $\Delta a \sim 0.4$ mm only shown for SiC50/PMMA as toughness data becomes "invalid" in terms of ASTM standards [34].)

4.3. Comparison to other structural ceramic materials

The present SiC/PMMA hybrid materials display at best crack-growth toughnesses (in stress intensity terms) that are 12 MPa m$^{0.5}$ (strictly ASTM valid values) and which approach 19 MPa m$^{0.5}$ for crack extensions that exceed the exclusion limit of $\Delta a \sim 0.4$ mm for our specimen dimensions. This is almost an order of magnitude tougher than commercial monolithic silicon carbide (Hexoloy SA), which is an extremely brittle ceramic with K_c toughness on the order of 2 MPa m$^{0.5}$ with no evidence of R-curve behavior.[4] Through the use of sintering additives to create nanoscale glassy films in the grain boundaries (so called "wet boundaries"), as in ABC-SiC [35,36], an intergranular (as opposed to transgranular) fracture can be achieved, and the resulting grain bridging induces a rising R-curve with crack-growth toughness approaching 9 MPa m$^{0.5}$, although the tensile strengths are significantly reduced to below 400 MPa. Our current SiC/PMMA hybrid materials display R-curve toughening behavior that even exceed these latter values for the toughest silicon carbide materials to date (Fig. 9), although with their lamellar architectures and significant

---

[4] Hexoloy SA, however, is very hard with excellent high-temperature capability. Tensile strengths can exceed 500 MPa at temperatures above 1600 °C, with compressive strengths even higher.

(40–60 vol.%) polymer contents they cannot display strength levels that can compete with these commercial materials.

Compared to other freeze-cast bio-inspired ceramics containing a "polymeric compliant phase", the current SiC/PMMA composites are certainly comparable in strength and R-curve toughness with the Al_2O_3/PMMA materials examined previously [6,25], but only for lamellar/dendritic structures. To achieve higher strengths and higher toughnesses in these materials, "brick-and-mortar" architectures offer a superior option. Indeed, in our previous studies using alumina scaffolds [6,25], Al_2O_3/PMMA materials containing 80 vol.% ceramic in "brick-and-mortar" configuration displayed R-curve toughnesses that were much higher – above 30 MPa $m^{0.5}$ – at strength levels of 200 MPa; however, the post freeze casting, cold pressing procedures needed to produce such "nacre-like" structures were found to be not feasible with the more brittle SiC scaffolds.

5. Conclusions

Freeze casting has been identified as a versatile processing route to fabricate nacre-inspired ceramic hybrid composites. We have shown here that we can manipulate the architecture of freeze-cast scaffolds at multiple length-scales by controlling processing parameters such as cooling rate and suspension solid content. However, as the influence of these parameters on the final scaffolds is rather complex, we simultaneously varied different factors to modify the desired structural features. This approach enabled us to fabricate scaffolds with ceramic fraction between 40 and 60 vol.%, having lamellae thicknesses over a wide range of 5–35 μm and exhibiting either lamellar or dendritic morphologies.

By coupling R-curve analysis with *in situ* observation of crack growth, we demonstrate that a fine tuning of the composites architecture through the control of processing parameters is fundamental to achieving the combination of properties typical of natural materials such as nacre. The mechanical behavior of our SiC/PMMA composites depends on the ceramic/polymer ratio, the layers thickness, and the presence of bridges that connect ceramic lamellae. All the samples investigated in this study show an increasing resistance to failure with crack propagation through both intrinsic toughening from plastic deformation in the polymer and interlayer regions, coupled with extrinsic toughening from a litany of mechanisms including lamellae pull-out, uncracked-ligament bridging, crack deflection, and ceramic bridge failures. In particular, this latter mechanism is observed to enhance both strength and toughness, akin to natural nacre where the presence of pre-existing mineral bridges acts to prevent debonding and to limit platelets sliding. SiC/PMMA samples characterized by a dendritic morphology benefit from this toughening mechanism, reaching values of toughness and strength higher than lamellar composites with same ceramic fraction.

Compared to commercially available monolithic silicon carbides and other comparable freeze-cast ceramic/compliant phase lamellar materials (specifically Al_2O_3/PMMA), the current SiC/PMMA composites with lamellar or dendritic architectures can display significantly higher R-curve toughness values, indeed at best higher than any silicon carbide ceramic to date. However, the more brittle SiC hybrid materials still cannot match the tensile strength levels of monolithic SiC's [35] nor the R-curve toughness of our previously reported Al_2O_3/PMMA hybrid materials with brick-and-mortar architectures [6,25].

Acknowledgments

This work was funded through the Mechanical Behavior of Materials Program at Lawrence Berkeley National Laboratory by the U.S. Department of Energy, Office of Science, Office of Basic Energy Sciences, Materials Sciences and Engineering Division, under Contract No. DE-AC02-05CH11231. The authors would like to thank Drs. Robert Kostecki and Jaroslaw Syzdek for allowing us access to their high-temperature furnace, and to Amy Wat for her assistance.

References

[1] R.O. Ritchie, The conflict between stress and toughness, Nat. Mater. 10 (2011) 817–822.
[2] U.G.K. Wegst, M.F. Ashby, The mechanical efficiency of natural materials, Philos. Mag. 84 (21) (2004) 2167–2181.
[3] M.E. Launey, R.O. Ritchie, On the fracture toughness of advanced materials, Adv. Mater. 21 (2009) 2103–2110.
[4] G.M. Luz, J.F. Mano, Biomimetic design of materials and biomaterials inspired by the structure of nacre, Philos. Trans. R. Soc. A 367 (2009) 1587–1605.
[5] C. Wang, Y. Huang, Q. Zan, H. Guo, S. Cai, Biomimetic structure design—a possible approach to change the brittleness of ceramics in nature, Mater. Sci. Eng. C 11 (2009) 9–12.
[6] E. Munch, M.E. Launey, D.H. Alsem, E. Saiz, A.P. Tomsia, R.O. Ritchie, Tough, bio-inspired hybrid materials, Science 322 (2008) 1516–1520.
[7] O.O. Ekiz, A.F. Dericioglu, H. Kakisawa, An efficient hybrid conventional method to fabricate nacre-like bulk nano-laminar composites, Mater. Sci. Eng. C 29 (2009) 2050–2054.
[8] M.E. Launey, E. Munch, D.H. Alsem, E. Saiz, A.P. Tomsia, R.O. Ritchie, A novel biomimetic approach to the design of high-performance ceramic–metal composites, J. R. Soc. Interface 7 (2010) 741–753.
[9] F. Bouville, E. Maire, S. Meille, B. Van de Moortèle, A.J. Stevenson, S. Deville, Strong, tough and stiff bioinspired ceramics from brittle constituents, Nat. Mater. 13 (2014) 508–514.
[10] A.P. Jackson, J.F.V. Vincent, R.M. Turner, The mechanical design of nacre, Proc. R. Soc. Lond. B 234 (1988) 415–440.
[11] A.G. Evans, Z. Suo, R.Z. Wang, I.A. Aksay, M.Y. He, J.W. Hutchinson, Model for the robust mechanical behavior of nacre, J. Mater. Res. 16 (9) (2001) 2475–2484.
[12] F. Barthelat, H. Tang, P.D. Zavattieri, C.M. Li, H.D. Espinosa, On the mechanics of mother-of-pearl: a key feature in the material hierarchical structure, J. Mech. Phys. Solids 55 (2007) 306–337.
[13] H.D. Espinosa, A. Juster, F.J. Latourte, O.Y. Loh, D. Gregoire, P.D. Zavattieri, Tablet-level origin of toughening in abalone shells and translation to synthetic composite materials, Nat. Commun. 2 (2011) 173.
[14] H.D. Espinosa, J.E. Rim, F. Barthelat, M. Buehler, Merger of structure and material in nacre and bone – perspectives on de novo biomimetic materials, Prog. Mater. Sci. 16 (2009) 1059–1100.
[15] M.R. Begley, N.R. Philips, B.G. Compton, D.V. Wilbrink, R.O. Ritchie, M. Utz, Micromechanical models to guide the development of synthetic 'brick and mortar' composites, J. Mech. Phys. Solids 60 (2012) 1545–1560.
[16] Y. Shao, H. Zhao, X. Feng, On flaw tolerance of nacre: a theoretical study, J. R. Soc. Interface 11 (2014) 20131016.
[17] F. Barthelat, Designing nacre-like materials for simultaneous stiffness, strength and toughness: optimum materials, composition, microstructure and size, J. Mech. Phys. Solids 73 (2014) 22–37.
[18] W.J. Clegg, K. Kendall, N.M. Alford, T.W. Button, J.D. Birchall, A simple way to make tough ceramics, Nature 347 (1990) 455–457.
[19] H. Kakisawa, T. Sumitomo, R. Inoue, Y. Kagawa, Fabrication of nature-inspired bulk laminar composites by a powder processing, Compos. Sci. Technol. 70 (2010) 161–166.
[20] Z. Tang, N.A. Kotov, S. Magonov, B. Ozturk, Nanostructured artificial nacre, Nat. Mater. 2 (6) (2003) 413–418.
[21] L.J. Bonderer, A.R. Studart, L.J. Gauckler, Bioinspired design and assembly of platelet reinforced polymer films, Science 319 (2008) 1069–1073.
[22] W. Cui, M. Li, J. Liu, B. Wang, C. Zhang, L. Jiang, Q. Cheng, A strong integrated strength and toughness artificial nacre based on dopamine cross-linked graphene oxide, ACS Nano 8 (9) (2014) 9511–9517.
[23] Y.G. Li, T. Yu, T.Y. Yang, L.X. Zheng, K. Liao, Bio-inspired nacre-like composite films based on graphene with superior mechanical, electrical, and biocompatible properties, Adv. Mater. 24 (2012) 3426–3431.
[24] S. Deville, E. Saiz, R.K. Nalla, A.P. Tomsia, Freezing as a path to build complex composites, Science 311 (2006) 515–518.
[25] M.E. Launey, E. Munch, D.H. Alsem, H.B. Barth, E. Saiz, A.P. Tomsia, R.O. Ritchie, Designing highly toughened hybrid composites through nature-inspired hierarchical complexity, Acta Mater. 57 (2009) 2919–2932.
[26] T. Fukusawa, M. Ando, T. Ohji, S. Kanzaki, Synthesis of porous ceramics with complex pore structure by freeze-dry processing, J. Am. Ceram. Soc. 84 (1) (2001) 230–232.
[27] S.R. Mukai, H. Nishihara, H. Tamon, Formation of monolithic silica gel microhoneycombs (SMHs) using pseudosteady state growth of microstructural ice crystals, Chem. Commun. 7 (2004) 874–875.
[28] H. Zhang, I. Hussain, M. Brust, M.F. Butler, S.P. Rannard, A.I. Cooper, Aligned two-and three-dimensional structures by directional freezing of polymers and nanoparticles, Nat. Mater. 4 (2005) 787–793.

[29] V. Naglieri, H.A. Bale, B. Gludovatz, A.P. Tomsia, R.O. Ritchie, On the development of ice-templated silicon carbide scaffolds for nature-inspired structural materials, Acta Mater. 61 (2013) 6948–6957.

[30] S. Berg, F.M. Parez, N. Ni, P.D.V. Pereira, R.C. Maher, E. Garcia-Tunon, S. Eslava, S. Agnoli, C. Mattevi, E. Saiz, Mesoscale assembly of chemically modified graphene into complex cellular networks, Nat. Commun. 5 (2014) 1–10.

[31] E. Munch, E. Saiz, A.P. Tomsia, S. Deville, Architectural control of freeze-cast ceramics through additives and templating, J. Am. Ceram. Soc. 92 (7) (2009) 1534–1539.

[32] S. Deville, G. Bernard-Granger, Influence of surface tension, osmotic pressure and pores morphology on the densification of ice-templated ceramics, J. Eur. Ceram. Soc. 31 (2011) 983–987.

[33] D20 Committee, D790-10 Standard Test Methods for Flexural Proprieties of Unreinforced and Reinforced Plastic and Electrical Insulating Materials, ASTM International, West Conshohocken, PA, 2010.

[34] E08 Committee, E1820-11E2 Standard Test Methods for Measurement of Fracture Toughness, ASTM International, West Conshohocken, PA, 2011.

[35] J.J. Cao, W.J. MoberlyChan, L.C. DeJonghe, C.J. Gilbert, R.O. Ritchie, In situ toughened silicon carbide with Al-B-C additions, J. Am. Ceram. Soc. 79 (2) (1996) 461–469.

[36] C.J. Gilbert, J.J. Cao, W.J. MoberlyChan, L.C. DeJonghe, R.O. Ritchie, Cyclic fatigue and resistance-curve behavior of an in situ toughened silicon carbide with Al-B-C additions, Acta Mater. 44 (1996) 3199–3214.